UNSW SYDNEY

CIRCLE-F/V: a dual-mode CRISPR-Cas13a cascade biosensor for ultrasensitive and visual detection of low-abundance EGFR mutations

Author:
Zhu, T; Wang, Z; Wu, Y; Jiang, W; Deng, F; Fang, R; Yang, D

Publication details:
Journal of Biological Engineering
v. 20
Chapter No. 1
Medium: Electronic
1754-1611 (ISSN)

Publication Date:
2026-12-01

Publisher DOI:
https://doi.org/10.1186/s13036-026-00675-4

Downloaded from http://hdl.handle.net/1959.4/107499 in https://unsworks.unsw.edu.au on 2026-08-20

Journal of Biological Engineering

https://doi.org/10.1186/s13036-026-00675-4

Article in Press

CIRCLE-F/V: a dual-mode CRISPR-Cas13a cascade biosensor for ultrasensitive and visual detection of low-abundance EGFR mutations

Received: 7 January 2026

Accepted: 24 March 2026

Published online: 27 March 2026

Cite this article as: Zhu T., Wang Z., Wu Y. *et al.* CIRCLE-F/V: a dual-mode CRISPR-Cas13a cascade biosensor for ultrasensitive and visual detection of low-abundance EGFR mutations. *J Biol Eng* (2026). https://doi.org/10.1186/s13036-026-00675-4

Tao Zhu, Zixuan Wang, Yingyu Wu, Weiwei Jiang, Fei Deng, Rong Fang & Danting Yang

We are providing an unedited version of this manuscript to give early access to its findings. Before final publication, the manuscript will undergo further editing. Please note there may be errors present which affect the content, and all legal disclaimers apply.

If this paper is publishing under a Transparent Peer Review model then Peer Review reports will publish with the final article.

ARTICLE IN PRESS

© The Author(s) 2026. **Open Access** This article is licensed under a Creative Commons Attribution-NonCommercial-NoDerivatives 4.0 International License, which permits any non-commercial use, sharing, distribution and reproduction in any medium or format, as long as you give appropriate credit to the original author(s) and the source, provide a link to the Creative Commons licence, and indicate if you modified the licensed material. You do not have permission under this licence to share adapted material derived from this article or parts of it. The images or other third party material in this article are included in the article's Creative Commons licence, unless indicated otherwise in a credit line to the material. If material is not included in the article's Creative Commons licence and your intended use is not permitted by statutory regulation or exceeds the permitted use, you will need to obtain permission directly from the copyright holder. To view a copy of this licence, visit http://creativecommons.org/licenses/by-nc-nd/4.0/.

ARTICLE IN PRESS

CIRCLE-F/V: A Dual-Mode CRISPR-Cas13a Cascade Biosensor for Ultrasensitive and Visual Detection of Low-abundance EGFR Mutations

Tao ZHU[1], Zixuan WANG[2], Yingyu WU[1], Weiwei JIANG[1], Fei DENG[3], Rong FANG[2**], Danting YANG[1**]

(1 School of Public health, Health Science Center, Ningbo University, 818 Fenghua Road, Ningbo, Zhejiang Province, 315211, People's Republic of China. 2 Ningbo Clinical Pathology Diagnosis Center, Ningbo, Zhejiang 315021, PR China. 3 ARC Centre of Excellence in Nanoscale Biophotonics, University of New South Wales, Sydney 2052)

** The corresponding authors contributed equally. E-mail: rachelrainyr@163.com; yangdanting@nbu.edu.cn

ARTICLE IN PRESS

ARTICLE IN PRESS

Abstract Precise identification of low-frequency EGFR L858R mutations is crucial for targeted therapy and prognosis in non-small cell lung cancer (NSCLC). Here, we present CIRCLE-F/V (CRISPR-based Integrated Restriction-assisted Cyclic Loop-mediated Enhancement Fluorescence/Visual platform), a dual-mode CRISPR-Cas13a cascade biosensor enabling ultrasensitive and specific mutation detection through integrated fluorescence and visual readouts. The system combines restriction-assisted mutant enrichment with cyclic CRISPR signal amplification. Genomic DNA is selectively digested with MscI to eliminate wild-type alleles, followed by T7 promoter–mediated PCR amplification and in vitro transcription. The resulting RNA activates Cas13a-crRNA complexes, initiating both direct reporter cleavage and dumbbell-triggered cascade amplification (DTCA) -mediated secondary signal enhancement. Under optimized conditions, the fluorescence mode achieved a variant allele frequency (VAF) sensitivity of 0.01%, with an estimated genomic DNA detection limit of ~3.6 fM in the integrated workflow and an RNA detection limit of ~2.16 pM. By replacing the fluorescent reporter with a FAM–biotin probe, the visual mode via lateral flow strips was realized with a VAF sensitivity of 0.01%. Clinical validation demonstrated complete concordance with next-generation sequencing (NGS), accurately classifying as high-, low-, and negative mutation samples. By integrating selective allele enrichment, cyclic amplification, and dual-mode readout, CIRCLE-F/V represents a sensitive, versatile, and clinically adaptable platform for rapid EGFR genotyping and early NSCLC screening.

Keywords CRISPR-Cas13a system, EGFR L858R mutation, dumbbell-triggered cascade amplification, fluorescence, lateral flow assay, biosensor

ARTICLE IN PRESS

1. Introduction

Lung cancer remains the leading cause of cancer-related mortality worldwide, accounting for more than two million deaths each year [1, 2]. Non-small cell lung cancer (NSCLC) represents approximately 85% of cases, with mutations epidermal growth factor receptor (EGFR) gene serving as key drivers of tumorigenesis and therapeutic response [3-6]. The L858R point mutation, a leucine-to-arginine substitution at codon 858 in exon 21 of the EGFR tyrosine kinase domain (c.2573T>G at the DNA level), represents one of the most prevalent activating mutations in non-small cell lung cancer (NSCLC) [7-10]. As a clinically actionable driver mutation, L858R alters the ATP-binding pocket of the EGFR kinase, leading to constitutive activation of downstream signaling pathways and conferring high sensitivity to EGFR tyrosine kinase inhibitors (TKIs) [7]. Consequently, the presence of this mutation directly determines patient eligibility for first-line targeted therapies. Because such mutations may occur at extremely low frequencies in heterogeneous tumor samples or liquid biopsies, precise identification at single-nucleotide resolution is essential. High-sensitivity detection is therefore critical to avoid false-negative results that could deprive patients of potentially life-extending TKI therapy, while also enabling early diagnosis and longitudinal disease monitoring. Conventional polymerase chain reaction (PCR) and its derivatives such as ARMS-PCR, digital droplet PCR (ddPCR), and peptide nucleic acids (PNA) clamping—have improved diagnostic sensitivity but remain limited by complex instrumentation, restricted dynamic range, and susceptibility to false positives [11, 12-16]. Next-generation sequencing (NGS) provides comprehensive genomic profiling yet demands costly equipment, long turnaround times, and lengthy data processing, hindering its application in routine or point-of-care testing (POCT) [11, 17-19]. Hence, there is an urgent need for rapid, accurate, and accessible platforms capable of detecting low-frequency EGFR mutations with single-nucleotide resolution.

ARTICLE IN PRESS

Clustered regularly interspaced short palindromic repeat (CRISPR) loci and their associated Cas nucleases constitute an adaptive immune system in prokaryotes. Although CRISPR arrays were first described in *Escherichia coli K12*, subsequent studies have demonstrated that CRISPR–Cas systems are widely distributed across diverse bacterial and archaeal species [20-22]. Leveraging their programmable sequence recognition and collateral cleavage activity, CRISPR-Cas-based platforms have rapidly emerged as powerful tools for nucleic acid detection [23, 24]. Among these, CRISPR-Cas systems have been extensively explored for identifying EGFR mutations, with Cas12a being the most widely employed nuclease for detecting the clinically significant L858R variant. For instance, Deng and colleagues developed ID-CRISPR, which integrates Cas12a with a DNA hydrogel matrix to detect rare mutant alleles with a sensitivity of 0.1% [25]. Similarly, Yuan's group designed a Cas12a crown nanomachine, enabling direct and highly sensitive detection of circulating tumor DNA and RNA in undiluted serum with a detection limit of 0.14 pM for EGFR L858R ctDNA [26]. Although CRISPR-based diagnostic platforms have demonstrated remarkable sensitivity, important mechanistic differences exist between Cas12a- and Cas13a-based systems. Cas12a primarily targets double-stranded DNA (dsDNA) and, upon recognition of a complementary DNA sequence containing a protospacer adjacent motif (PAM), activates collateral cleavage of non-target single-stranded DNA (ssDNA) reporters. While this property enables signal amplification, the strict PAM requirement and DNA substrate dependence may limit flexibility in detecting single-nucleotide variants. In addition, performance can be influenced by DNA template complexity in complex biological samples [27-29]. In contrast, the CRISPR–Cas13a specifically recognizes RNA substrates. Upon target RNA binding by the Cas13a–crRNA complex, conformational activation of the HEPN domains triggers robust collateral cleavage of non-target single-stranded RNA (ssRNA) reporters. This RNA-guided recognition mechanism allows precise single-nucleotide discrimination without PAM constraints. Importantly, coupling

ARTICLE IN PRESS

upstream transcription with Cas13a activation enables efficient cascade amplification, whereby a single recognition event generates amplified chemical signals. These characteristics confer high sensitivity, broad target compatibility, and enhanced suitability for detecting clinically relevant single-nucleotide mutations [30-33].

Conventional CRISPR-Cas13a assays relying solely on a single crRNA–Cas13a system and a simple ssRNA–FQ reporter often fail to detect ultra-low-abundance single-nucleotide variants, owing to limited *trans*-cleavage turnover and weak signal amplification. To overcome these inherent constraints, additional isothermal or cascade amplification modules are typically required to enhance detection sensitivity [34]. CRISPR-Cas detection platforms are frequently coupled with isothermal amplification techniques, such as RPA, LAMP, and HDA, to enhance analytical sensitivity. Although these methods offer rapid amplification without thermocycling, they may suffer from non-specific amplification, primer-dependent artifacts, and increased false-positive rates [35-39]. To address these limitations, structurally engineered probes, including hairpin- and dumbbell-based designs, have been incorporated into CRISPR diagnostic systems to achieve programmable signal regulation and cascade amplification [40-42]. However, hairpin probes may exhibit background leakage due to spontaneous structural opening, and previously reported dumbbell-based designs often involve complex preparation procedures or limited cascade integration. In contrast, the present DTCA-assisted CIRCLE-F/V platform integrates a rationally engineered dumbbell-triggered cascade amplification architecture with restriction-assisted mutant enrichment and dual-mode signal output, enabling enhanced sensitivity and mutation discrimination. Moreover, single-mode biosensors—based on either fluorescence or colorimetric outputs—are prone to false negatives and offer limited analytical depth when distinguishing single-base mismatches [43].

ARTICLE IN PRESS

To overcome these limitations, we developed CIRCLE-F/V (CRISPR-based Integrated Restriction-assisted Cyclic Loop-mediated Enhancement Fluorescence/Visual platform), a stepwise signal amplification system based on CRISPR-Cas13a. The platform enables highly specific detection of the EGFR L858R mutation via an integrated workflow combining restriction enzyme–mediated mutant enrichment, DTCA probe–mediated cascade amplification, and dual-mode signal readout. By integrating front-end wild-type depletion with modular fluorescence and lateral-flow visual readouts, CIRCLE-F/V achieves ultrasensitive mutation detection in complex biological matrices. The innovation of CIRCLE-F/V lies in its dumbbell-triggered cascade amplification (DTCA) module, which couples programmable Cas13a *trans*-cleavage with a cyclic signal regeneration process, markedly boosting detection sensitivity without complex instrumentation. Additionally, selective digestion of wild-type EGFR alleles by MscI effectively suppresses background interference, ensuring single-nucleotide-level specificity. Under optimized conditions, CIRCLE-F/V achieves femtomolar-level detection and discriminates mutant allele frequencies as low as 0.01% (fluorescence) and 0.01% (visual). CIRCLE-F/V integrates high sensitivity, dual-mode flexibility, and operational simplicity, offering a novel and clinically adaptable diagnostic platform for EGFR genotyping and early NSCLC mutation screening.

ARTICLE IN PRESS

2. Materials and Methods

2.1 Materials and Apparatus

All oligonucleotides, including PCR primers, crRNAs, DTCA probes, RNA fluorescence (5'-FAM/3'-BHQ1) or visual (5'-FAM/3'-biotin) reporters, were synthesized and HPLC-purified by General Biol (Anhui, China). Detailed sequences and chemical modifications are listed in Table S1. CRISPR-Cas13a protein was purchased from Beijing Kexin Biotech (Beijing, China), and the T7 in vitro transcription kit from Thermo Fisher Scientific (Beijing, China). DNA gel extraction and RNA purification kits were purchased from Omega Bio-Tek

ARTICLE IN PRESS

(USA) and Autobio Engineering (Shanghai, China), respectively. DsRNA Ladder was obtained from Beijing Quanshijin Biotechnology (Beijing, China). Another marker (Item No. N0363S), capable of resolving lower molecular weights, was obtained from New England Biolabs (Beijing, China). RNA markers and the restriction enzyme MscI were supplied by New England Biolabs (Beijing, China). RNase inhibitor, T4 RNA ligase 2, and RNase R were obtained from MedChemExpress (Shanghai, China), Hanhai New Enzyme (Wuhan, China), and Beyotime Biotechnology (Shanghai, China), respectively. Cas12/13-specific nucleic acid lateral flow strips (catalog no. JY0301) were purchased from Beijing Baoying Tonghui Biotechnology Co., Ltd. (Beijing, China). The DNA extraction kit (catalog no. RC1102) is from Kaishuo Biotechnology (Xiamen) Co., Ltd. (Xiamen, China).

Polyacrylamide gel electrophoresis (PAGE) was performed using a Bio-Rad vertical electrophoresis system (Bio-Rad Laboratories, CA, USA), and gels were visualized on a 5200-imaging system (Tianneng Technology, Shanghai, China). Nucleic acid concentrations were determined using a NanoDrop One spectrophotometer (Thermo Fisher Scientific, MA, USA). DNA concentration and total mass were measured using a Qubit 4.0 fluorometer (Q33226; Thermo Fisher Scientific, MA, USA). Fluorescence measurements were conducted on a LightCycler 480 II real-time PCR instrument (Roche Diagnostics, Basel, Switzerland) and a WL-16-III constant-temperature fluorescence detector (Anpu Future Biotechnology, Changzhou, China). Lateral flow test strips were supplied by Beijing Baoying Tonghui Biotechnology Co., Ltd. (Beijing, China).

ARTICLE IN PRESS

2.2 DNA Processing, In Vitro Transcription, and RNA Purification

Clinical DNA samples representing multiple *EGFR* genotypes were obtained with informed consent under approval from the Ningbo Clinical Pathological Diagnosis Center (approval number: NBPC-NBSZ202501). Wild-type *EGFR* DNA was selectively digested with MscI at 37 ℃ for 60 min, followed by heat inactivation at 80 ℃ for 20 min. Digestion efficacy was

ARTICLE IN PRESS

verified by agarose gel electrophoresis, and the desired bands were excised and purified. For the preparation of T7 transcription template, PCR amplification was performed using an upstream primer containing a T7 promoter and a conventional downstream primer. Purified PCR products were transcribed in vitro using T7 RNA polymerase at 37 ℃ for 1 h, followed by DNase I treatment at 37 ℃ for 15 min to remove template DNA. The reaction was terminated with 0.5 M EDTA, and RNA was purified and concentrated using a spin-column kit. RNA integrity and concentration was confirmed with NanoDrop analysis.

2.3 Preparation of DNA Samples with Defined Mutation Frequencies

To prepare samples with defined *EGFR* L858R mutation frequencies of 10%, 1%, 0.5%, 0.1%, and 0.01%, wild-type DNA (500 ng) was mixed with 50 ng, 5 ng, 2.5 ng, 0.5 ng, and 0.05 ng of mutant DNA, respectively. All mixtures were prepared using nuclease-free water and stored at -20 ℃ until use.

2.4 Preparation of Dumbbell-Triggered Cascade Amplification (DTCA) Probes

Single-stranded RNA (ssRNA) was heated to 90℃ for 1 minute and gradually cooled to 25 ℃ (-0.1 ℃ every 5 s) to allow annealing. The resulting product was ligated with T4 RNA ligase 2 in the presence of 50% PEG 8000 and RNase inhibitor at 25 ℃ for 4 h. The reaction was quenched with 0.5 M EDTA and purified, then treated with RNase R at 37 ℃ for 10 min to remove linear RNA species, followed by heat inactivation at 70 ℃ for 10 min. Formation of the closed dumbbell structure was confirmed by non-denaturing PAGE and quantified by Nanodrop analysis.

2.5 CRISPR-Cas13a Fluorescence Detection

Cas13a protein was pre-incubated with either crRNA-L or crRNA-C at a 1.5:1 molar ratio at 37 ℃ for 25 min to form the respective Cas13a-crRNA-L and Cas13a-crRNA-C ribonucleoprotein complexes. Each 20 µL reaction

ARTICLE IN PRESS

contained target RNA, DTCA probes, FQ reporters, reaction buffer, and RNase inhibitor. Real-time fluorescence signals were recorded at 39 ℃ for 90 minutes using a Roche LightCycler 480 II system. CrRNA screening experiments were additionally validated using the WL-16-III fluorescence detector.

2.6 CRISPR-Cas13a Visual Detection via Lateral Flow Assay

For point-of-care visual detection, reactions were performed as described above using FAM-biotin-labeled RNA reporters instead of FQ probes. After 30 min of incubation at 39 ℃, 50 μL of the reaction mixture was applied to a commercial lateral flow strip. Results were read within 10 min. The presence of both the control (C) and test (T) line indicated a positive result, while only a C line signified a negative sample.

2.7 Data Analysis

All experiments were performed in triplicate. Data were presented as the mean ± SEM. Statistical significance was assessed using two-tailed Student's t-tests ($P < 0.05$) with GraphPad Prism 10 (GraphPad Software, La Jolla, CA, USA). Grayscale analysis of test strip images was performed using ImageJ software.

ARTICLE IN PRESS

3. Results and Discussion

3.1 Principle and Feasibility of the CIRCLE-F/V Technology Platform

The CIRCLE-F/V platform establishes a cascade signal amplification framework that leverages the collateral cleavage activity of CRISPR-Cas13a for ultrasensitive and specific detection of the clinically relevant *EGFR* L858R point mutation in NSCLC. As illustrated in Fig.1, genomic DNA is first digested with the restriction enzyme MscI, which selectively cleaved wild-type *EGFR* sequences while leaving the mutant allele intact, thereby minimizing background interference (Fig. S1). The undigested mutant templates are then

ARTICLE IN PRESS

amplified by PCR, during which a T7 promoter is incorporated to enable subsequent transcription into RNA using a T7 polymerase system. The resulting RNA transcripts serve as substrates for Cas13a-mediated recognition and *trans*-cleavage.

The detection mechanism involves two Cas13a-crRNA ribonucleoprotein (RNP) complexes, --crRNA-L and crRNA-C to establish a dual-layer cascade. Upon recognition of the L858R mutant RNA, the Cas13a-crRNA-L complex is activated, initiating *trans*-cleavage of both a fluorophore-quencher (FQ) reporter and a dumbbell-triggered cascade amplification (DTCA) probe containing a "-UU-" motif. Cleavage of the DTCA probe releases two ssRNA fragments complementary to crRNA-C sequence, which subsequently activate additional Cas13a-crRNA-C complexes. This cyclic activation process generates multiple rounds of FQ probe cleavage, producing a robust and self-reinforcing fluorescence signal for sensitive mutation detection. For point-of-care testing (POCT), the same mechanism is translated into a visual detection mode using a FAM–biotin dual-labeled RNA probe integrated with lateral flow strips. In the absence of the mutation, Cas13a remains inactive and the intact FAM–biotin probe binds colloidal gold–anti-FAM antibodies, producing a red signal only at the control (C) line. In contrast, the presence of the L858R mutation activates Cas13a, cleaving the FAM–Biotin probe and liberating FAM fragments that bypass the C line and are captured at the test line, generating a visible red signal (Fig.1). The intensity and pattern of the T and C lines thus enable rapid, instrument-free determination of mutation status.

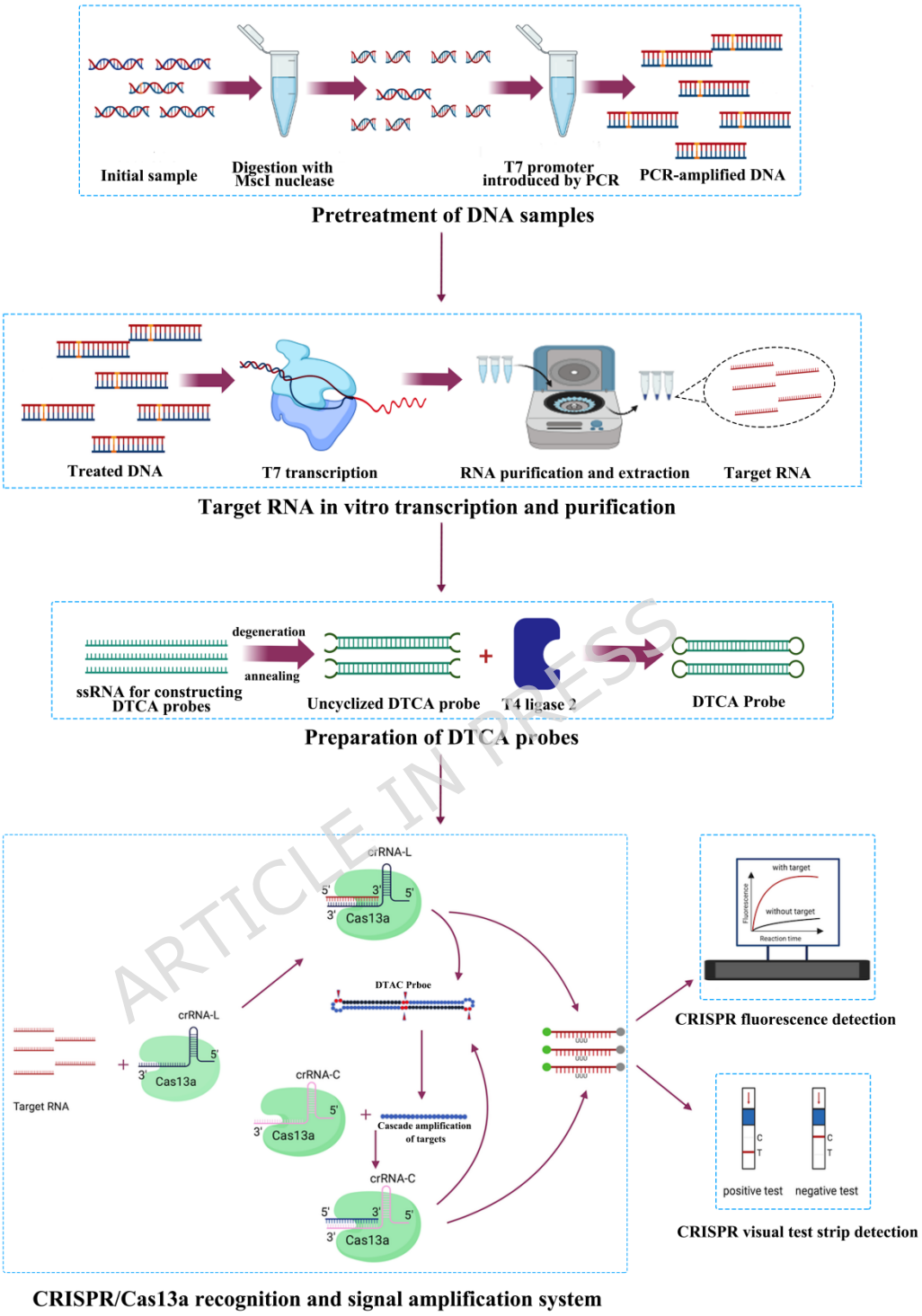

Fig. 1 Schematic illustration of the CIRCLE-F/V technology platform based on CRISPR-Cas13a for the detection of EGFR L858R mutation

To evaluate the feasibility of the CIRCLE-F/V system, six reaction conditions were examined: (a) no target RNA and no DTCA probe; (b) DTCA

ARTICLE IN PRESS

probe only (no target RNA); (c) mutant RNA + DTCA probe; (d) wild-type RNA + DTCA probe; (e) mutant RNA without DTCA probe; and (f) wild-type RNA without DTCA probe. As shown in the kinetic traces (Figure 2A-i), the baseline condition (a) exhibits negligible fluorescence, indicating minimal background signal, while the DTCA-only condition (b) shows only slight probe leakage. The mutant RNA + DTCA probe group (c) displays a pronounced fluorescence increase (~800 RFU), whereas the wild-type RNA + DTCA probe group (d) remains at a substantially lower level (<200 RFU). Comparison between mutant RNA with and without DTCA (c vs e) reveals a marked signal enhancement introduced by the DTCA probe. Importantly, comparison between wild-type conditions with and without DTCA (d vs f) shows that wild-type signals remain consistently low, indicating that DTCA amplification does not increase nonspecific background. These results demonstrate that DTCA-mediated signal amplification is strictly dependent on specific Cas13a activation. In combination with upstream MscI digestion, this dual-gating mechanism enables high-fidelity single-nucleotide discrimination. Endpoint analysis (Figure 2A-ii) further confirms that DTCA significantly broadens the diagnostic window ($F_{mut} \gg F_{wt}$), allowing clear differentiation between mutant and wild-type targets.

To isolate the effect of DTCA on Cas13a *trans*-cleavage output, three reaction compositions were compared (Figure 2B): (a) Cas13a–crRNA + target RNA + DTCA + FQ reporter; (b) Cas13a–crRNA + target RNA + FQ reporter (without DTCA); and (c) Cas13a–crRNA + FQ reporter only. Fluorescence was quantified as $\Delta F = F_t - F_0$, where F_t represents real-time fluorescence and F_0 represents the initial fluorescence. Inclusion of DTCA (condition a) resulted in a steeper initial slope and a higher endpoint ΔF compared with the non-amplified system (condition b), corresponding to an approximately fourfold increase at 80 minutes (Figure 2B-i, ii). Condition (c) remained at baseline, confirming that fluorescence output requires reporter cleavage and that ΔF reflects Cas13a

ARTICLE IN PRESS

trans-cleavage activity. Taken together with the wild-type data in Figure 2A, these results suggest that DTCA serves as an efficient cascade amplifier rather than a passive signal enhancer. It markedly accelerates signal generation for mutant targets without a proportional increase in wild-type background, thereby improving the signal-to-background ratio relative to the non-amplified system. Non-denaturing PAGE analysis (Figure 2C) revealed a discrete band corresponding to the DTCA probe, clearly distinct from the linear ssRNA control. The increased electrophoretic mobility and compact band pattern are consistent with successful dumbbell circularization. The absence of additional bands indicates high purity of the circular product and supports its role as a stable amplification trigger.

To evaluate the restriction step, mixed-allele samples (0.01–10% VAF) were analyzed with or without MscI digestion prior to CRISPR detection. Readouts are reported as ΔI/I (%), where I_0 is the initial fluorescence, I is the final fluorescence and $\Delta I = I - I_0$. Across all VAFs, MscI pretreatment markedly increased ΔI/I for mutation-positive mixtures while suppressing background from wild-type alleles (Fig. 2D); improvements were statistically significant (****, $P<0.0005$). Notably, the post-digest ΔI/I values scale with VAF, expanding the dynamic range from low-abundance (0.01%) to high-abundance (10%) samples and confirming that restriction digestion is a critical specificity gate in the CIRCLE workflow.

ARTICLE IN PRESS

ARTICLE IN PRESS

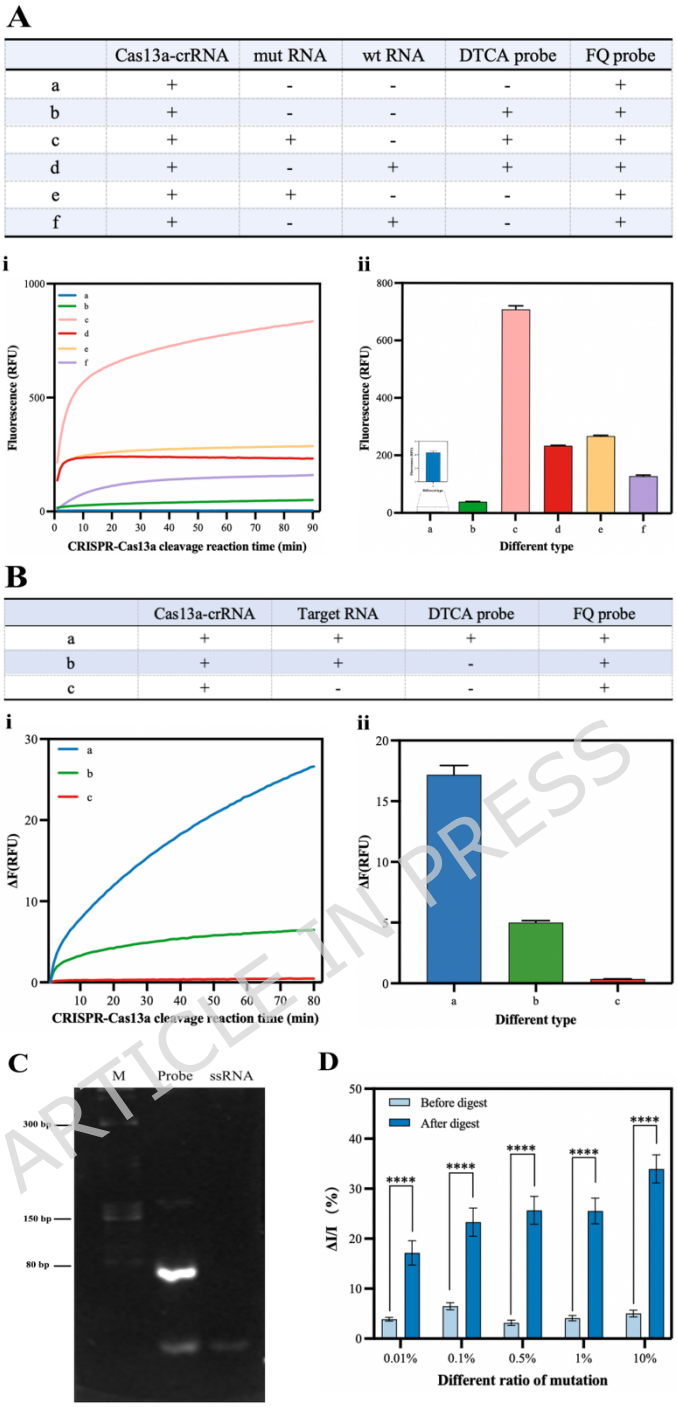

Fig. 2 Validation of the CRISPR-Cas13a-based assay. (A) Validation of the CRISPR-Cas13a fluorescence detection assay. (i) Fluorescence intensity curve; (ii) Fluorescence signal bar chart. (B) Evaluation of signal amplification mediated by the DTCA probe. (i) Fluorescence intensity curve; (ii) Fluorescence signal bar chart. (C) PAGE analysis of the DTCA probe. M: RNA Ladder; Probe: DTCA probe. (D) ΔI/I values before and after treatment with MscI restriction enzyme. Statistical significance: **** $P < 0.0005$.

ARTICLE IN PRESS

3.2 Optimization of Experimental Parameters

To maximize the analytical performance of the CIRCLE-F/V platform for detecting the EGFR L858R mutation, key biochemical and reaction parameters were systematically optimized. Parameters examined included crRNA design, Cas13a–crRNA pre-assembly conditions, enzyme concentration, ribonucleoprotein (RNP) stoichiometry, and reaction temperature.

3.2.1 Optimization of crRNA design

Previous studies have shown that the location of a mismatch within the crRNA spacer strongly affects both target recognition and single-nucleotide discrimination efficiency [44, 45]. Guided by this principle, five candidate crRNAs were designed with the L858R mutation positioned at different spacer sites (Fig. 3A(i)). Each crRNA was tested against wild-type and mutant EGFR templates to evaluate signal output and background leakage. As summarized in the fluorescence heatmap (Fig. 3A-ii), crRNA4 produced the highest fluorescence for the mutant target while maintaining minimal signal for the wild-type, yielding the best signal-to-noise ratio. The superior performance of crRNA4 is likely attributed to its mutation recognition site lying outside the seed region (nucleotides 9–15 from the 5′ end), preserving optimal base-pairing and efficient Cas13a activation. In contrast, mismatches located within or adjacent to the seed region in the other crRNAs likely disrupted target binding and impaired *trans*-cleavage efficiency [30]. Therefore, crRNA4 was selected for all subsequent experiments.

3.2.2 Optimization of RNP assembly and reaction conditions

Efficient assembly of Cas13a–crRNA RNP complexes is crucial for rapid activation and strong fluorescence output [46]. The effects of pre-incubation time, enzyme concentration, and molar ratio were therefore systematically evaluated.

As shown in Fig. 3B, fluorescence intensity increased progressively with

ARTICLE IN PRESS

longer pre-incubation, reaching a plateau at 25 min (37 ℃), indicating complete RNP formation. Beyond 25 min, no significant improvement was observed, suggesting equilibrium binding between Cas13a and crRNA [47, 48].

Cas13a concentration was next optimized from 10 to 400 nM (Fig. 3C). Fluorescence intensity rose sharply up to 100 nM, beyond which the signal slightly decreased, possibly due to substrate depletion or steric interference between enzyme complexes. Therefore, 100 nM was determined as the optimal Cas13a concentration.

Finally, the molar ratio of Cas13a to crRNA was adjusted between 2:1 and 1:2 (2:1, 1.5:1, 1:1, 1:1.5, and 1:2). A ratio of 1.5:1 produced the strongest fluorescence response, whereas excess Cas13a or crRNA reduced cleavage efficiency (Fig. 3D), which is consistent with previous findings [46, 49]. This configuration was thus adopted for all subsequent assays to ensure maximal catalytic efficiency and consistent signal generation.

ARTICLE IN PRESS

ARTICLE IN PRESS

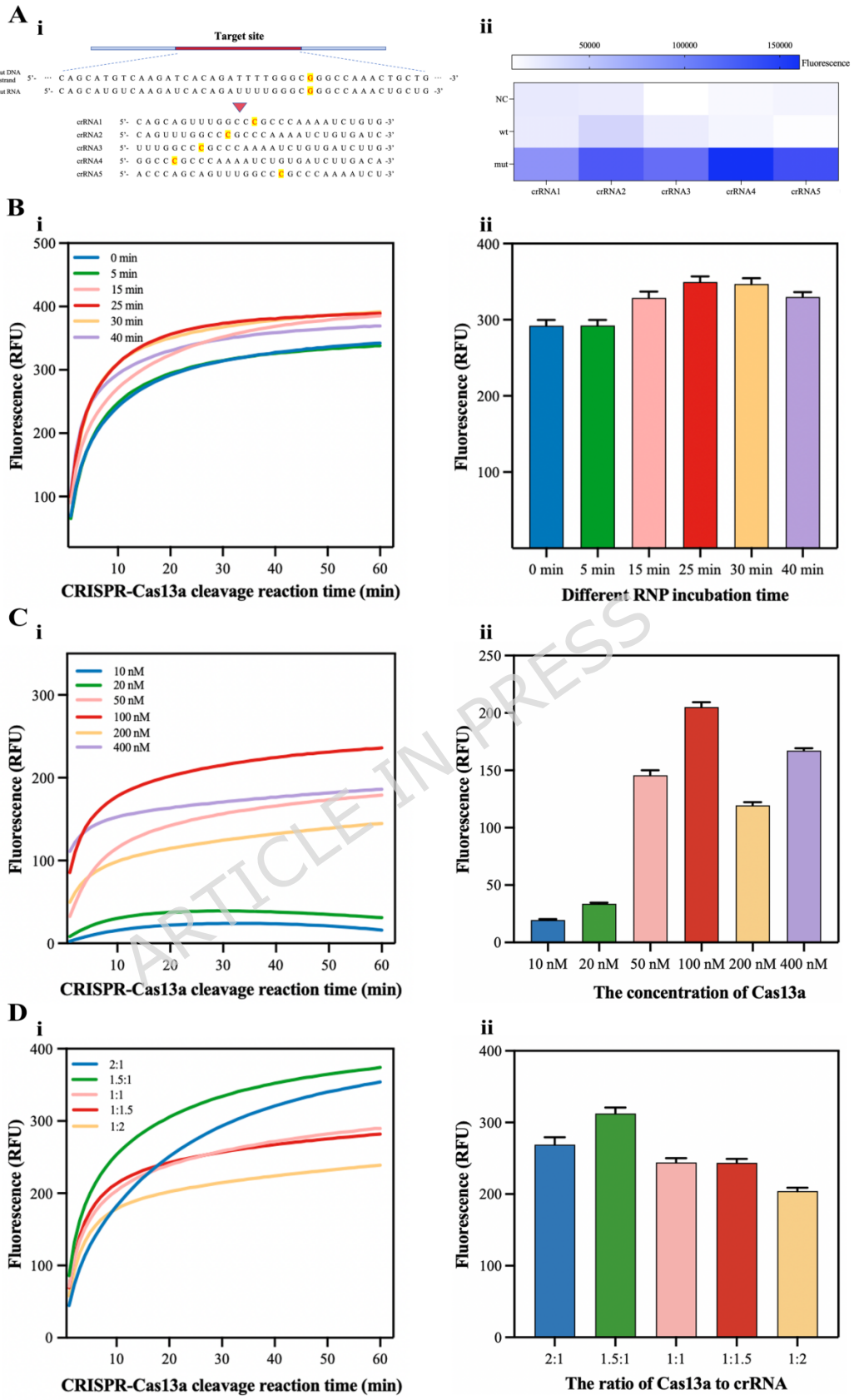

Fig. 3 Optimization of experimental conditions. (A) Design and screening of crRNAs. (i) Schematic illustration of crRNA design targeting the EGFR L858R

ARTICLE IN PRESS

mutation site; (ii) Heatmap showing the results of crRNA specificity screening. (B) Optimization of ribonucleoprotein (RNP) incubation time. (i) Fluorescence intensity curve; (ii) Fluorescence signal bar chart. (C) Determination of optimal Cas13a concentration. (i) Fluorescence intensity curve; (ii) Fluorescence signal bar chart. (D) Evaluation of the Cas13a-to-crRNA ratio. (i) Fluorescence intensity curve; (ii) Fluorescence signal bar chart.

3.2.3 Optimization of reaction temperature and probe concentrations

Reaction temperature exerts a critical influence on Cas13a conformational dynamics and catalytic efficiency [50, 51]. To determine the optimal temperature for *trans*-cleavage, reactions were performed from 35 ℃ to 45 ℃ under otherwise identical conditions. As shown in Fig. 4A, fluorescence intensity increased with temperature and peaked at 39 ℃, indicating maximal enzyme activity and target recognition at this point (Fig. 4A). Temperatures above 40 °C caused a modest signal decline, likely due to partial denaturation of the crRNA–target duplex. Consequently, 39 ℃ was selected as the optimal reaction temperature for all subsequent assays.

Next, the FQ reporter concentration was optimized over a range of 100–4000 nM [46, 52]. The optimal FQ reporter concentration was evaluated using the signal-to-noise ratio (S/N), defined as the fluorescence intensity of the 858R mutant divided by that of the blank control. As shown in Figure 4B, the S/N ratio increased rapidly as the probe concentration rose from 100 nM to 2000 nM and reached a stable plateau after 30 minutes of reaction. Although the 4000 nM group exhibited slightly higher absolute S/N values, its kinetic curve (Figure 4B-i) displayed greater signal fluctuations and did not reach a stable plateau throughout the reaction. Considering the need for stable diagnostic signals, strong background suppression in complex clinical matrices, and the diminishing benefits of increasing FQ reporter concentration from 2000 nM to 4000 nM, the optimal FQ reporter concentration was thus set at 2000 nM.

ARTICLE IN PRESS

To further enhance the amplification cascade, the concentration of the DTCA probe was optimized from 50 to 1000 nM. As shown in Fig. 4C, Signal gain ($\Delta I/I_0$) increased proportionally up to 500 nM and then reached a plateau, implying saturation of the secondary amplification step. Thus, 500 nM DTCA was adopted as the optimal condition for subsequent assays.

After integrating these parameters, the final optimized reaction mixture contained 100 nM Cas13a, 66.7 nM crRNA4, 500 nM DTCA probe, and 2000 nM FQ probe. The complexes were pre-incubated at 37 ℃ for 25 min, followed by detection at 39 ℃ using a real-time PCR platform. Under these optimized conditions, the CIRCLE-F/V assay exhibited rapid signal accumulation and high reproducibility, providing a robust basis for subsequent analytical and clinical evaluations.

ARTICLE IN PRESS

ARTICLE IN PRESS

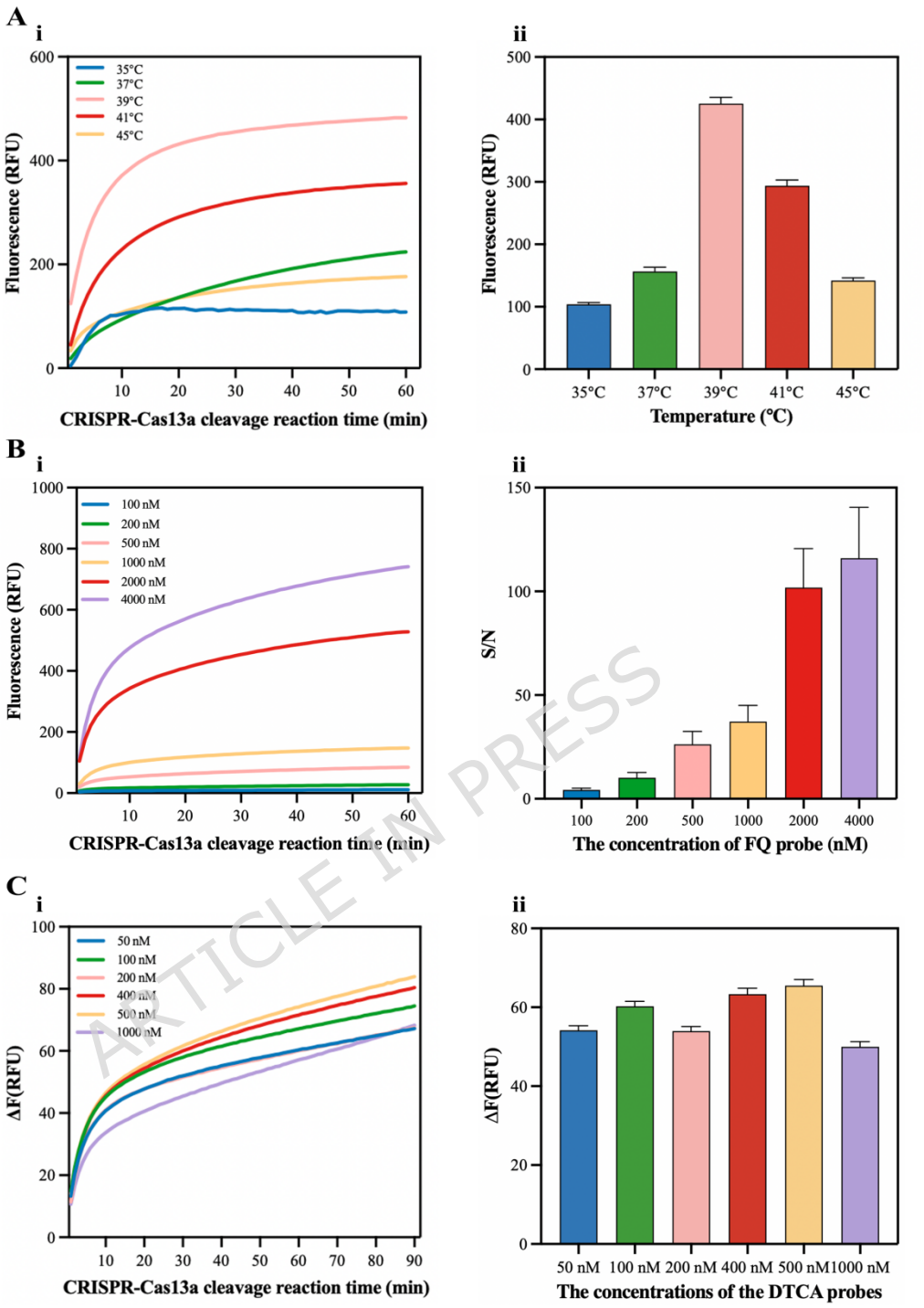

Fig 4. Optimization of Reaction Temperature and Probe Concentrations for the CIRCLE-F Detection Platform. (A) Optimization of the reaction temperature for CRISPR-Cas13a trans-cleavage activity. (i) Fluorescence intensity curves of CRISPR-Cas13a at different reaction temperatures; (ii) Corresponding bar plots of fluorescence intensity at different reaction

ARTICLE IN PRESS

temperatures. (B) Determination of the optimal concentration of fluorescent reporting probes in the CIRCLE-F detection method. (i) Dynamics curves of signal-to-noise ratio obtained using fluorescent reporting probes of different concentrations; (ii) Bar charts corresponding to signal-to-noise ratios at different reported probe concentrations. (C) Determination of the optimal concentration of the DTCA probe for the CIRCLE-F detection method.(i) Fluorescence intensity curves obtained with DTCA probes at different concentrations; (ii) Corresponding bar plots of fluorescence intensity at different DTCA probe concentrations.

3.3 Analytical Performance of the CIRCLE-F/V Platform

The analytical performance of the CIRCLE-F/V platform for detecting the *EGFR* L858R mutation was evaluated under optimized reaction conditions.

3.3.1 Sensitivity

As shown in Figure 5A, fluorescence intensity increased proportionally with target RNA concentrations ranging from 1 to 10,000 pM, demonstrating a wide dynamic range. A strong linear relationship was observed between the relative fluorescence change (ΔI/I) and the logarithmic concentration of target RNA, with a regression equation of $Y = 24.33X - 3.892$ ($R^2 = 0.9301$) (Figure 5B). A calibration curve was constructed by plotting fluorescence intensity against the $\log_{10}$-transformed RNA concentration. The limit of detection (LOD) was calculated in the logarithmic domain using the 3×SD/slope method according to: $LOD_{log} = 3 \times SD/k$. where SD represents the standard deviation of blank measurements and k denotes the slope of the calibration curve. The calculated logarithmic LOD was 0.3343, corresponding to $\log_{10}(C_{LOD})$. The LOD in absolute concentration units was obtained by inverse logarithmic

ARTICLE IN PRESS

transformation: $C_{LOD}=10^{LOD_{log}}$, yielding an RNA LOD of 2.16 pM. This value represents the intrinsic analytical sensitivity of the Cas13a detection module toward RNA targets. Because genomic DNA samples require PCR amplification and in vitro transcription prior to Cas13a detection, the genomic DNA detection limit was not directly measured. Instead, it was estimated based on the experimentally determined RNA LOD and the amplification efficiency of the upstream reactions. Repeated experiments demonstrated a stable upstream amplification efficiency of approximately 600-fold. Accordingly, the estimated genomic DNA LOD was 3.6 fM. This value represents the theoretical sensitivity of the integrated workflow rather than a directly measured analytical detection limit. Ultimately, these results confirm the femtomolar sensitivity of the system and highlight the ultrasensitive performance of the CIRCLE-F/V platform.

3.3.2 Detection of low-frequency variants

Given the clinical relevance of variant allele frequencies (VAFs) in NSCLC management [34, 53], we further evaluated the platform's ability to detect rare mutant alleles. DNA mixtures containing L858R mutation frequencies of 10%, 1%, 0.5%, 0.1%, and 0.01% were analyzed. As shown in Fig. 5C, the CIRCLE-F/V platform achieved a VAF sensitivity of 0.01%. According to previously published reports, conventional PCR-CRISPR/Cas13a detection methods typically achieve a minimum detectable mutation frequency of approximately 0.1% VAF [54-56], while most NGS-based approaches detect mutations at ≥1% VAF [57]. These comparisons indicate that the CIRCLE-F/V platform provides enhanced relative to representative conventional approaches reported in the literature. This high sensitivity enhancement highlights the benefit of

ARTICLE IN PRESS

integrating DTCA-mediated amplification into the Cas13a system.

3.3.3 Dual-mode visualization and point-of-care applicability

To adapt the system for rapid point-of-care detection, the FQ reporter was replaced with a FAM–biotin dual-labeled RNA probe compatible with lateral flow strips (Fig. 5D and Table S2). Figure 5D-i schematically illustrates the working principle of the lateral flow strip in the CIRCLE-F/V visual mode. Specifically, the conjugate pad contains colloidal gold-labeled anti-FAM monoclonal antibodies. The control line (C line) is coated with streptavidin, and the test line (T line) is coated with sheep anti-mouse secondary antibodies. The sample migrates along the strip via capillary action, sequentially passing the conjugate pad, control line, test line, and absorbent pad. In the absence of target RNA, the CRISPR–Cas13a system remains inactive and the FAM-biotin reporter stays intact. The intact reporter binds the gold-labeled anti-FAM antibody via the FAM moiety, forming a gold–antibody-reporter complex. Upon reaching the control line, the biotin moiety binds streptavidin, immobilizing the intact reporter complex at the control line. Due to the strong biotin-streptavidin interaction and steric stabilization, the complex does not migrate further to the test line. As a result, gold nanoparticles accumulate at the control line, producing a visible control signal, which is interpreted as a negative result. When target RNA is present, activated Cas13a cleaves the reporter into FAM-labeled and biotion-labled fragments. The FAM-containing fragments remain associated with the gold-labeled anti-FAM antibody and migrate beyond the control line, while biotin-containing fragments are captured at the C line. The gold–anti-FAM antibody complexes are subsequently captured at the test line by the anti-mouse secondary antibodies, producing a visible test signal. Complete reporter cleavage results in a test-line signal only, whereas partial cleavage may yield both control and test signals. Therefore, the presence of a test-line signal (with or without a control-line signal) is interpreted as a positive result. Therefore, in this study, the T and C lines of the strip enabled intuitive

ARTICLE IN PRESS

visual interpretation within minutes. Wild-type samples yielded only a C line, whereas mutant samples at ≥ 0.5% VAF produced clear T lines, whose intensity scaled with mutation frequency. Even at 0.01% VAF, a faint but distinguishable T line was observed, setting the visual detection threshold at 0.01% VAF ((Fig 5D(ii)). Grayscale quantification (Image J) yielded mean T/C ratios of 0.65 for wild-type, 0.98 for 0.01% mutant, and > 1.0 for all higher mutation levels, with T/C ≥ 0.98 defined as the diagnostic cutoff for positive mutation identification.

3.3.4 Specificity and reproducibility

Assay specificity was assessed against potentially interfering genomic variants, including *EGFR* 19del (mutant and wild-type), *KRAS* G12C (mutant and wild-type), and *ALK* fusion–positive templates (each 1 nM). As shown in Fig. 5E, only the L858R mutant generated a strong signal, while all other variants remained near background, demonstrating excellent single-nucleotide specificity. The accuracy and precision of the CIRCLE-F/V workflow were assessed across multiple independent runs using EGFR L858R RNA samples spanning a concentration range of 1-1000 pM. The coefficient of variation (CV) for both intra- and inter-batch measurements was below 8%, indicating high repeatability of the platform within the tested picomolar concentration range (Table 1.1). Additionally, experimental accuracy and reproducibility of CIRCLE-F/V platform samples at different VAF levels were evaluated using a uniform target concentration of 2 pM. Variations measured within and between groups did not exceed 8% (Table 1.2). These results indicate that the quantitative performance of RNA detection remains consistent under the tested conditions. Notably, the detection limit (3.6 fM) for genomic DNA at the femtomolar level represents a theoretical estimate derived from the experimentally determined RNA LOD (2.16 pM) and the calculated upstream amplification efficiency.

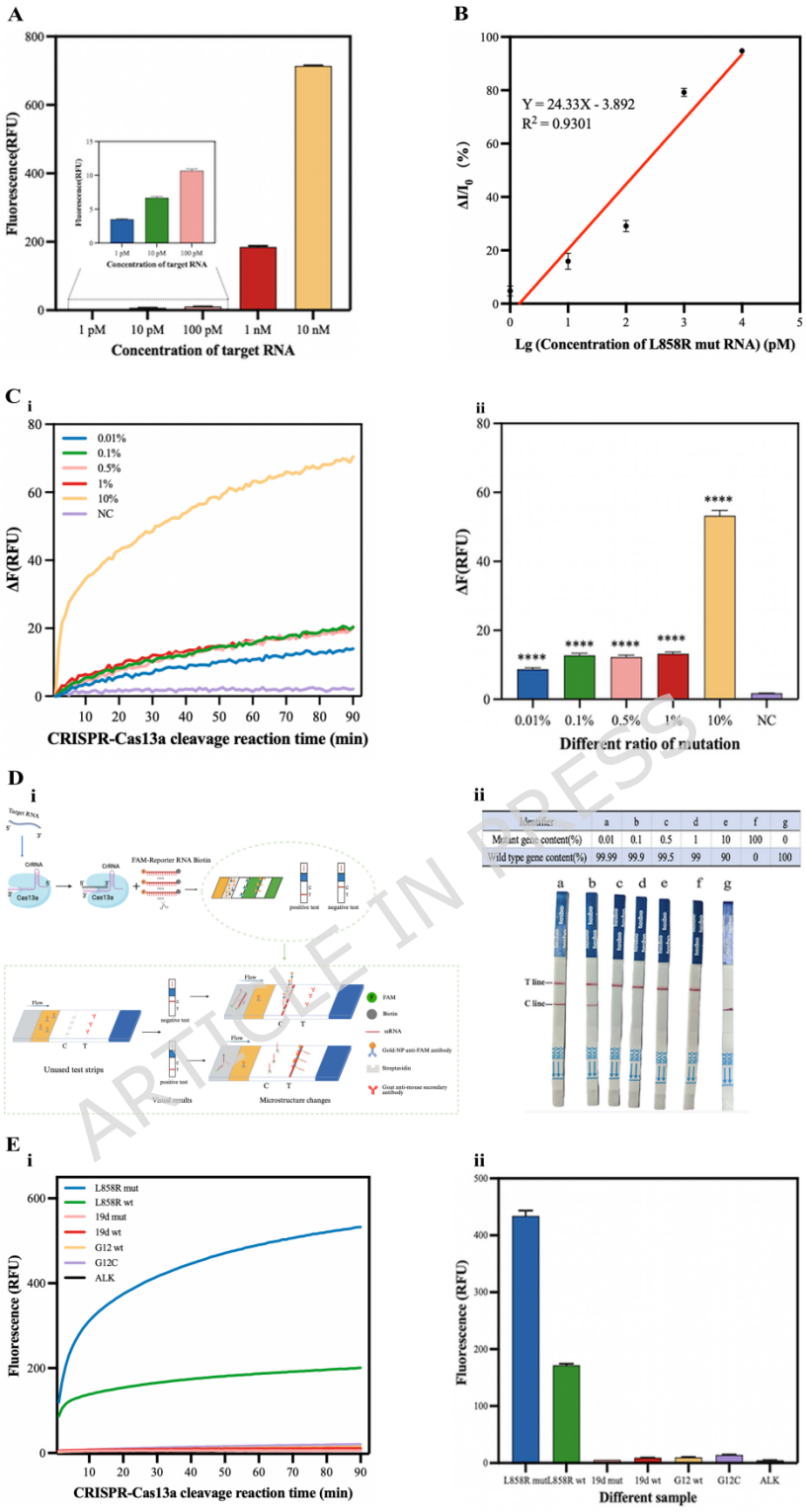

Fig 5. Performance evaluation of the CIRCLE-F/V technology. (A) Fluorescence intensity at varying concentrations of the target RNA. (B) Calibration curve constructed from the logarithmic concentration of the target RNA versus $\Delta I/I_0$. (C) Detection of different mutation frequencies. (i)

ARTICLE IN PRESS

Fluorescence intensity curves; (ii) Bar chart of fluorescence signal intensity. Statistical significance: ***P < 0.0005. (D) Detection performance of the CIRCLE-F/V visual detection mode. (i) Schematic illustration of the working principle of the test strip in the CIRCLE-F/V visual detection mode; (ii) Visual detection results of genes with different mutation frequencies using the CIRCLE-F/V mode. (E) Specificity analysis of the CIRCLE-F/V technology for detecting different gene variants. (i) Fluorescence intensity curves; (ii) Bar chart of fluorescence signal intensity.

Table 1.1 Repeated experiments at different concentrations

Sample concentration (pM)	Coefficient of variation (%)	
	Intra-group (%)	Inter-group (%)
10^0	3.03	2.89
10^1	3.00	0.59
10^2	6.59	3.99
10^3	4.28	7.39
Negative control	7.40	2.60

ARTICLE IN PRESS

Table 1.2 Repeated experiments across different VAF levels

Variable allele frequency (%)	Coefficient of variation (%)	
	Intra-group (%)	Inter-group (%)
0.01	7.81	6.91
0.1	2.62	2.01
0.5	4.56	4.39
1	4.92	1.75
10	3.60	2.01

ARTICLE IN PRESS

NC	7.05	3.17

Most previously reported fluorescence-based assays achieve either a low detection limit or the ability to discriminate low variant allele frequencies (VAFs), but rarely both (Table 2). In contrast, the CIRCLE-F/V system developed here uniquely combines femtomolar-level sensitivity (3.63 fM) with precise discrimination of rare alleles (0.01% VAF in fluorescence mode and 0.1% in visual mode) while offering dual readouts—quantitative fluorescence and qualitative lateral flow visualization. By integrating a dumbbell-triggered cascade amplification (DTCA) with Cas13a-mediated trans-cleavage, CIRCLE-F/V enhances both analytical versatility and clinical applicability, demonstrating the potential of Cas13a-based diagnostics for precision lung cancer genotyping.

ARTICLE IN PRESS

ARTICLE IN PRESS

Table 2 A comparison of representative CRISPR-Cas platforms developed for EGFR L858R mutation detection

Biosensor	CRISPR-Cas type	Signal output mode	Detection limit	The lowest detected mutation frequency	References
PER-CRISPR-Cas14a electrochemical biosensor	CRISPR-Cas14a	Electrochemical mode	0.34 fM	N.A.	[6]
BM-TOA system	CRISPR-Cas12a	Fluorescence mode	N.A.	0.1%	[58]
CRISPR-Cas12a Corona Nanomachine	CRISPR-Cas12a	Fluorescence mode	0.14 pM	N.A.	[26]
CASMART	CRISPR-Cas12a	Fluorescence mode	3 copies·μL^{-1}	0.1%	[59]
HiCASE	CRISPR-Cas13a	Fluorescence mode	N.A.	0.01%	[12]
CIRCLE-F/V	CRISPR-Cas13a	Fluorescence mode&Visual mode	3.63 fM	0.01%(Fluorescence) 0.01%(Vision)	This work

ARTICLE IN PRESS

ARTICLE IN PRESS

3.4 Application of CIRCLE-F/V in Clinical Samples

To validate the clinical feasibility of the CIRCLE-F/V platform, its performance was benchmarked against NGS, the current gold standard for EGFR genotyping (Figure 6A). A total of 11 clinical DNA samples were obtained from the Ningbo Clinical Pathology Center, including seven EGFR L858R–positive and four wild-type cases. According to NGS analysis, Samples 1 and 2 exhibited the highest mutation frequencies (10.85% and 10.57%), followed by samples 3 and 4 (9.42% and 9.91%), samples 5 and 6 (4.90% and 5.99%), and sample 7 with the lowest abundance (2.31%), whereas samples 8–11 were confirmed as mutation-negative (0 %). Detailed NGS information for clinical samples, including sample sources, sequencing methodology is provided in Section 2 of Supplementary Information "*2. Clinical Sample Collection and NGS Analysis*".

3.4.1 Fluorescence mode (CIRCLE-F)

As shown in Fig. 6B, the fluorescence assay accurately classified all 11 samples, with fluorescence signals correlating strongly with the NGS-derived mutation frequencies. The CIRCLE-F results demonstrated full concordance with NGS, confirming that the platform can reliably distinguish between high-, low-, and non-mutant samples.

3.4.2 Visual mode (CIRCLE-V)

Lateral flow strip analysis was performed to evaluate the clinical applicability of the CIRCLE-F/V platform (Figure 6C). For mutation-positive samples (1-7), distinct red bands were observed on both the control (C) and test (T) lines, and T-line intensity correlated with NGS-derived mutation abundance. For samples 8–11, which were classified as wild-type by NGS, faint T-line signals were occasionally observed likely due to nonspecific adsorption of gold nanoparticles. However, quantitative grayscale analysis using ImageJ demonstrated that all corresponding T/C ratios remained below the predefined

ARTICLE IN PRESS

diagnostic threshold (0.65), and these samples were therefore classified as negative. To minimize subjectivity, per-sample T/C ratios for all clinical specimens are provided in Supplementary Table S4. All mutation-positive samples exhibited T/C values >0.65, whereas samples 8–11 were below this threshold. NGS designation of samples 8–11 as "0% VAF" indicates mutant read counts below the reporting threshold (20) and below the assay LOD (1%) under high-depth sequencing conditions. While variants below this threshold cannot be completely excluded, the weak T-line signals observed in these samples are most likely attributable to background adsorption or stochastic signal variation rather than confirmed low-frequency mutations. As shown in Figure 6D, fluorescence-mode results and quantitative visual-mode classification were concordant with NGS findings, supporting the reliability of the defined diagnostic threshold.

ARTICLE IN PRESS

ARTICLE IN PRESS

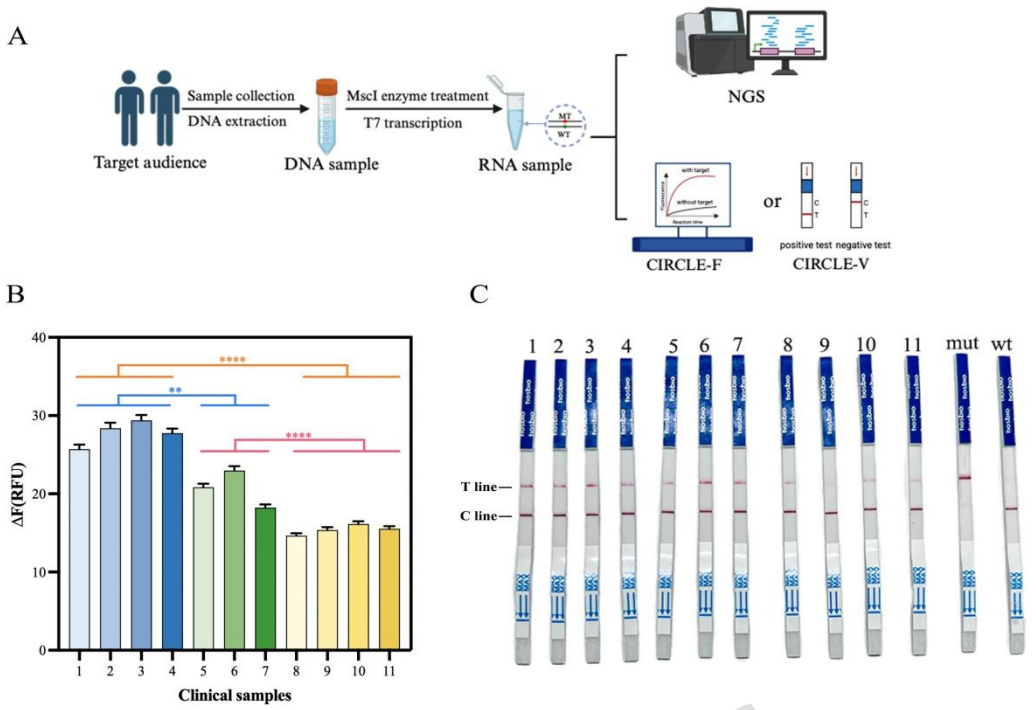

D

Screening Tset		NGS		Total	Sensitivity	Specificity
		WT	MT			
CIRCLE-F	MT	7	0	7	100%	100%
	WT	0	4	4		
	Total	7	4	11		
CIRCLE-V	MT	7	0	7	100%	100%
	WT	0	4	4		
	Total	7	4	11		

ARTICLE IN PRESS

Fig. 6 Detection of clinical samples using the CIRCLE-F/V detection platform. (A)Schematic diagram illustrating the workflow of NGS and CIRCLE-F/V analyses for detecting cancer mutations in patient clinical samples. (B) Fluorescence-based detection of 11 clinical samples using the CIRCLE-F/V platform, from left to right, experimental groups 1-4 (blue) represent high-mutation samples, groups 5-7 (green) represent low-mutation samples, and groups 8-11 (yellow) correspond to wild-type samples. **** $P < 0.0005$; ** $P < 0.05$. (C) Visual signal detection performance of the CIRCLE-F/V platform across 11 clinical samples, Among these, samples 1–4 constitute the high-mutation group, samples 5–7 constitute the low-mutation group, and samples

ARTICLE IN PRESS

8–11 represent the wild-type group. (D) This study compares the sensitivity and specificity of NGS, CIRCLE-F, and CIRCLE-V for identifying L858R mutations.

4. Conclusion

In summary, we developed a CRISPR-Cas13-based cyclic signal amplification system, termed CIRCLE-F/V, which employs dumbbell-shaped triple cascade amplification (DTCA) probes for ultrasensitive detection of EGFR L858R point mutations in lung cancer. By replacing conventional fluorescent reporters with FAM–biotin-labeled probes, the platform also enables convenient and intuitive visual readout via lateral flow strips. Compared with conventional PCR and next-generation sequencing (NGS) methods, CIRCLE-F/V exhibits higher sensitivity and specificity, improved repeatability, and user-friendly operation, making it well suited for resource-limited settings. Under optimized conditions, the fluorescence mode enables rapid and sensitive detection of genomic DNA at an estimated cost of approximately $2.3 per sample. The fluorescence mode exhibits a dynamic detection range of 1–10,000 pM for the L858R mutation, with an estimated theoretical detection limit of 3.6 fM for genomic DNA samples, and enables reliable identification of low-frequency variants with variant allele frequencies (VAFs) as low as 0.01%. The visual mode enables convenient detection of mutations in genomic DNA, with an estimated cost of approximately $4.5 per sample and a VAF sensitivity of 0.01%. Validation using clinical samples demonstrates that CIRCLE-F/V fluorescence detection accurately classifies samples into high-mutation, low-mutation, and mutation-negative groups, showing complete concordance with NGS results. The lateral flow test strip allows rapid discrimination between positive and negative samples. These findings highlight the clinical applicability and translational potential of the CIRCLE-F/V platform for diagnostic applications. In addition, the platform can be readily reconfigured to detect other target mutations by simply replacing

ARTICLE IN PRESS

the corresponding crRNA. Collectively, these features establish CIRCLE-F/V as a universal and practical tool for lung cancer genotyping, as well as a promising approach for sensitive and convenient mutation detection in both clinical and field settings.

ARTICLE IN PRESS

ARTICLE IN PRESS

References

[1] Bray F, Laversanne M, Sung H, et al. Global cancer statistics 2022: GLOBOCAN estimates of incidence and mortality worldwide for 36 cancers in 185 countries. CA Cancer J Clin, 2024, 74(3): 229-263. https://doi.org/10.3322/caac.21834

[2] Tesfaw L M, Dessie Z G, Mekonnen Fenta H. Lung cancer mortality and associated predictors: systematic review using 32 scientific research findings. Front Oncol, 2023, 13,1308897. https://doi.org/10.3389/fonc.2023.1308897

[3] O'kane G M, Bradbury P A, Feld R, et al. Uncommon EGFR mutations in advanced non-small cell lung cancer. Lung Cancer, 2017, 109, 137-144. https://doi.org/10.1016/j.lungcan.2017.04.016

[4] Aly R M, Serya R a T, El-Motwally A M, et al. Novel quinoline-3-carboxamides (Part 2): Design, optimization and synthesis of quinoline based scaffold as EGFR inhibitors with potent anticancer activity. Bioorg Chem, 2017, 75, 368-392. https://doi.org/10.1016/j.bioorg.2017.10.018

[5] Wang H Y, Liao W Y, Ho C C, et al. Enhanced detection of actionable mutations in NSCLC through pleural effusion cell-free DNA sequencing: A prospective study. Eur J Cancer, 2025, 217, 115224. https://doi.org/10.1016/j.ejca.2025.115224

[6] Qi J, Qi Q, Zhou Z, et al. PER-CRISPR-Cas14a system-based electrochemical biosensor for the detection of ctDNA EGFR L858R. Anal Methods, 2023, 16(1): 51-61. https://doi.org/10.1039/d3ay01615c

[7] Lynch T J, Bell D W, Sordella R, et al. Activating mutations in the epidermal growth factor receptor underlying responsiveness of non-small-cell lung cancer to gefitinib. N Engl J Med, 2004, 350(21): 2129-2139. https://doi.org/10.1056/NEJMoa040938

ARTICLE IN PRESS

[8] Li A R, Chitale D, Riely G J, et al. EGFR mutations in lung adenocarcinomas: clinical testing experience and relationship to EGFR gene copy number and immunohistochemical expression. J Mol Diagn, 2008, 10(3): 242-248. https://doi.org/10.2353/jmoldx.2008.070178

[9] Pecci F, Cantini L, Metro G, et al. Non-small-cell lung cancer: how to manage EGFR-mutated disease. Drugs Context, 2022, 11. https://doi.org/10.7573/dic.2022-4-1

[10] Meriggi F, Zaniboni A. Epidermal growth factor receptor tyrosine kinase inhibitors for elderly patients with advanced non-small cell lung cancer. Curr Gerontol Geriatr Res, 2010; 2010 (1): 348174. https://doi.org/10.1155/2010/348174

[11] Baba K, Fujita T, Tasaka S, et al. Simultaneous Detection of the T790M and L858R Mutations in the EGFR Gene by Oligoribonucleotide Interference-PCR. Int J Mol Sci, 2019, 20(16): 115224. https://doi.org/10.3390/ijms20164020

[12] Wang L, Wen X, Yang Y, et al. CRISPR-Cas13a-based supersensitive circulating tumor DNA assay for detecting EGFR mutations in plasma. Commun Biol, 2024, 7(1): 657. https://doi.org/10.1038/s42003-024-06368-2

[13] Siggillino A, Ulivi P, Pasini L, et al. Detection of EGFR Mutations in Plasma Cell-Free Tumor DNA of TKI-Treated Advanced-NSCLC Patients by Three Methodologies: Scorpion-ARMS, PNAClamp, and Digital PCR. Diagnostics (Basel), 2020, 10(12): 1062. https://doi.org/10.3390/diagnostics10121062

[14] Li C, He Q, Liang H, et al. Diagnostic Accuracy of Droplet Digital PCR and Amplification Refractory Mutation System PCR for Detecting EGFR Mutation in Cell-Free DNA of Lung Cancer: A Meta-Analysis. Front Oncol, 2020, 10, 290. https://doi.org/10.3389/fonc.2020.00290

ARTICLE IN PRESS

[15] Dominguez P L, Kolodney M S. Wild-type blocking polymerase chain reaction for detection of single nucleotide minority mutations from clinical specimens. Oncogene, 2005, 24(45): 6830-6834. https://doi.org/10.1038/sj.onc.1208832

[16] Nagai Y, Miyazawa H, Huqun, et al. Genetic heterogeneity of the epidermal growth factor receptor in non-small cell lung cancer cell lines revealed by a rapid and sensitive detection system, the peptide nucleic acid-locked nucleic acid PCR clamp. Cancer Res, 2005, 65(16): 7276-7282. https://doi.org/10.1158/0008-5472.CAN-05-0331

[17] Saito Y, Takahashi N, Matsui A, et al. Comparative study of the loop-mediated isothermal amplification method and the QIAGEN therascreen PCR kit for the detection of EGFR mutations in non-small cell lung cancer. J Thorac Dis, 2021, 13(2): 743-753. https://doi.org/10.21037/jtd-20-2642

[18] Long S. In pursuit of sensitivity: Lessons learned from viral nucleic acid detection and quantification on the Raindance ddPCR platform. Methods, 2022, 201: 82-95. https://doi.org/10.1016/j.ymeth.2021.04.008

[19] Wang L, Guo Q, Yu W, et al. Quantification of plasma EGFR mutations in patients with lung cancers: Comparison of the performance of ARMS-Plus and droplet digital PCR. Lung Cancer, 2017, 114: 31-37. https://doi.org/10.1016/j.lungcan.2017.10.007

[20] Ishino Y, Shinagawa H, Makino K, et al. Nucleotide sequence of the iap gene, responsible for alkaline phosphatase isozyme conversion in Escherichia coli, and identification of the gene product. J Bacteriol, 1987, 169(12): 5429-5433. https://doi.org/10.1128/jb.169.12.5429-5433.1987

[21] Nakata A, Amemura M, Makino K. Unusual nucleotide arrangement with repeated sequences in the Escherichia coli K-12 chromosome. J Bacteriol, 1989, 171(6): 3553-3556. https://doi.org/10.1128/jb.171.6.3553-3556.1989

ARTICLE IN PRESS

[22] Jansen R, Embden J D, Gaastra W, et al. Identification of genes that are associated with DNA repeats in prokaryotes. Mol Microbiol, 2002, 43(6): 1565-1575. https://doi.org/10.1046/j.1365-2958.2002.02839.x

[23] Del Giovane S, Bagheri N, Di Pede A C, et al. Challenges and perspectives of CRISPR-based technology for diagnostic applications. TrAC Trends in Analytical Chemistry, 2024, 172: 117594. https://doi.org/10.1016/j.trac.2024.117594

[24] Ghouneimy A, Mahas A, Marsic T, et al. CRISPR-Based Diagnostics: Challenges and Potential Solutions toward Point-of-Care Applications. ACS Synth Biol, 2023, 12(1): 1-16. https://doi.org/10.1021/acssynbio.2c00496

[25] Deng A, Mao Z, Jin X, et al. ID-CRISPR: A CRISPR-Cas12a platform for label-free and sensitive detection of rare mutant alleles using self-interference DNA hydrogel reporter. Biosens Bioelectron, 2025, 278, 117309. https://doi.org/10.1016/j.bios.2025.117309

[26] Yuan A, Sun T, Chen L, et al. CRISPR-Cas12a Corona Nanomachine for Detecting Circulating Tumor Nucleic Acids in Serum. Anal Chem, 2024, 96(50): 20074-20081. https://doi.org/10.1021/acs.analchem.4c04993

[27] Ai J, Deng J, Hu J, et al. PAM-Independent CRISPR-Cas12a System for Specific Assays of Single Nucleotide Variants. JACS Au, 2025, 5(3): 1392-1401. https://doi.org/10.1021/jacsau.5c00011

[28] Chen J S, Ma E, Harrington L B, et al. CRISPR-Cas12a target binding unleashes indiscriminate single-stranded DNase activity. Science, 2018, 360(6387): 436-439. https://doi.org/10.1126/science.aar6245

[29] Liu S, Rao X, Zhao R, et al. The trans DNA cleavage activity of Cas12a provides no detectable immunity against plasmid or phage. Front Genome Ed, 2022, 4, 929929. https://doi.org/10.3389/fgeed.2022.929929

ARTICLE IN PRESS

ARTICLE IN PRESS

[30] Kohabir K, Sistermans E, Wolthuis R. Recent advances in CRISPR-based single-nucleotide fidelity diagnostics. Communications Medicine, 2025, 5(1): 252. https://doi.org/10.1038/s43856-025-00933-4

[31] Zakiyyah S N, Sima K S P, Kharismasari C Y, et al. CRISPR-Cas13a-Powered Electrochemical Biosensors for RNA-based Disease Diagnostic and Monitoring. Sensors and Actuators Reports, 2025, 100358. https://doi.org/10.1016/j.snr.2025.100358

[32] Allemailem K S, Rahmani A H, Almansour N M, et al. Current updates on the structural and functional aspects of the CRISPR-Cas13 system for RNA targeting and editing: A next-generation tool for cancer management (Review). Int J Oncol, 2025, 66(5): 1-21. https://doi.org/10.3892/ijo.2025.5748

[33] Zhang J, You Y. CRISPR-Cas13a system: a novel approach to precision oncology. Cancer Biology & Medicine, 2020, 17(1): 6. https://doi.org/10.20892/j.issn.2095-3941.2019.0325

[34] Kellner M J, Koob J G, Gootenberg J S, et al. SHERLOCK: nucleic acid detection with CRISPR nucleases. Nat Protoc, 2019, 14(10): 2986-3012. https://doi.org/10.1038/s41596-019-0210-2

[35] Lai M Y, Lau Y L. Two-Stage Detection of Plasmodium spp. by Combination of Recombinase Polymerase Amplification and Loop-Mediated Isothermal Amplification Assay. Am J Trop Med Hyg, 2022, 107(4): 815-819. https://doi.org/10.4269/ajtmh.22-0136

[36] Moon Y J, Lee S Y, Oh S W. A Review of Isothermal Amplification Methods and Food-Origin Inhibitors against Detecting Food-Borne Pathogens. Foods, 2022, 11(3): 322. https://doi.org/10.3390/foods11030322

[37] Tan M, Liang L, Liao C, et al. A rapid and ultra-sensitive dual readout platform for Klebsiella pneumoniae detection based on RPA-CRISPR-Cas12a.

ARTICLE IN PRESS

Front Cell Infect Microbiol, 2024, 14, 1362513. https://doi.org/10.3389/fcimb.2024.1362513

[38] De Falco M, Colella S, Abdelkarim J a Y, et al. Helicase-dependent isothermal amplification turns biosensing into modern diagnostic technologies. Microchemical Journal, 2025, 114772. https://doi.org/10.1016/j.microc.2025.114772

[39] Barreda-Garcia S, Miranda-Castro R, De-Los-Santos-Alvarez N, et al. Helicase-dependent isothermal amplification: a novel tool in the development of molecular-based analytical systems for rapid pathogen detection. Anal Bioanal Chem, 2018, 410(3): 679-693. https://doi.org/10.1007/s00216-017-0620-3

[40] Zhong J, Xu Z, Peng J, et al. A CRISPR-Cas13a system based on a dumbbell-shaped hairpin combined with DNA-PAINT to establish the DCP-platform for highly sensitive detection of Hantaan virus RNA. Talanta, 2025, 291, 127852. https://doi.org/10.1016/j.talanta.2025.127852

[41] Chen D, Sun M, Li B, et al. Cascade CRISPR-Cas Enables More Sensitive Detection of Toxoplasma gondii and Listeria monocytogenes than Single CRISPR-Cas. Microorganisms, 2025, 13(8): 1896. https://doi.org/10.3390/microorganisms13081896

[42] Rossetti M, Merlo R, Bagheri N, et al. Enhancement of CRISPR-Cas12a trans-cleavage activity using hairpin DNA reporters. Nucleic Acids Res, 2022, 50(14): 8377-8391. https://doi.org/10.1093/nar/gkac578

[43] Ullah N, Bruce-Tagoe T A, Asamoah G A, et al. Multimodal Biosensing of Foodborne Pathogens. Int J Mol Sci, 2024, 25(11): 5959. https://doi.org/10.3390/ijms25115959

[44] Bai X, Gao P, Qian K, et al. A Highly Sensitive and Specific Detection Method for Mycobacterium tuberculosis Fluoroquinolone Resistance

ARTICLE IN PRESS

Mutations Utilizing the CRISPR-Cas13a System. Front Microbiol, 2022, 13, 847373. https://doi.org/10.3389/fmicb.2022.847373

[45] Yang Y, Sun L, Zhao J, et al. Improving trans-cleavage activity of CRISPR-Cas13a using engineered crRNA with a uridinylate-rich 5'-overhang. Biosens Bioelectron, 2024, 255, 116239. https://doi.org/10.1016/j.bios.2024.116239

[46] Hu F, Liu Y, Zhao S, et al. A one-pot CRISPR-Cas13a-based contamination-free biosensor for low-cost and rapid nucleic acid diagnostics. Biosens Bioelectron, 2022, 202, 113994. https://doi.org/10.1016/j.bios.2022.113994

[47] Feng W, Peng H, Zhang H, et al. A Sensitive Technique Unravels the Kinetics of Activation and Trans-Cleavage of CRISPR-Cas Systems. Angew Chem Int Ed Engl, 2024, 63(22): e202404069. https://doi.org/10.1002/anie.202404069

[48] De Silva P I T, Hiniduma K, Canete R, et al. Multiplexed CRISPR Assay for Amplification-Free Detection of miRNAs. Biosensors (Basel), 2025, 15(6): 346. https://doi.org/10.3390/bios15060346

[49] Hsieh K, Zhao G, Wang T H. Applying biosensor development concepts to improve preamplification-free CRISPR-Cas12a-Dx. Analyst, 2020, 145(14): 4880-4888. https://doi.org/10.1039/d0an00664e

[50] Mahas A, Marsic T, Lopez-Portillo Masson M, et al. Characterization of a thermostable Cas13 enzyme for one-pot detection of SARS-CoV-2. Proc Natl Acad Sci U S A, 2022, 119(28): e2118260119. https://doi.org/10.1073/pnas.2118260119

[51] Wang F, Zhang C, Xu H, et al. Structural Basis for the Ribonuclease Activity of a Thermostable CRISPR-Cas13a from Thermoclostridium caenicola. J Mol Biol, 2023, 435(17): 168197. https://doi.org/10.1016/j.jmb.2023.168197

ARTICLE IN PRESS

[52] Ding X, Yin K, Li Z, et al. Ultrasensitive and visual detection of SARS-CoV-2 using all-in-one dual CRISPR-Cas12a assay. Nat Commun, 2020, 11(1): 4711. https://doi.org/10.1038/s41467-020-18575-6

[53] Casula M, Pisano M, Paliogiannis P, et al. Comparison between Three Different Techniques for the Detection of EGFR Mutations in Liquid Biopsies of Patients with Advanced Stage Lung Adenocarcinoma. Int J Mol Sci, 2023, 24(7): 6410. https://doi.org/10.3390/ijms24076410

[54] Zhou W, Yang J, Zhang Y, et al. Current landscape of gene-editing technology in biomedicine: Applications, advantages, challenges, and perspectives. MedComm (2020), 2022, 3(3): e155. https://doi.org/10.1002/mco2.155Digital Object Identifier

[55] Palacin-Aliana I, Garcia-Romero N, Carrion-Navarro J, et al. ddPCR Overcomes the CRISPR-Cas13a-Based Technique for the Detection of the BRAF p.V600E Mutation in Liquid Biopsies. Int J Mol Sci, 2024, 25(20): 10902. https://doi.org/10.3390/ijms252010902

[56] Amintas S, Cullot G, Boubaddi M, et al. Integrating allele-specific PCR with CRISPR-Cas13a for sensitive KRAS mutation detection in pancreatic cancer. J Biol Eng, 2024, 18(1): 53. https://doi.org/10.1186/s13036-024-00450-3

[57] Jing C, Mao X, Wang Z, et al. Next-generation sequencing-based detection of EGFR, KRAS, BRAF, NRAS, PIK3CA, Her-2 and TP53 mutations in patients with non-small cell lung cancer. Mol Med Rep, 2018, 18(2): 2191-2197. https://doi.org/10.3892/mmr.2018.9210

[58] Wu Y, Luo W, Weng Z, et al. A PAM-free CRISPR-Cas12a ultra-specific activation mode based on toehold-mediated strand displacement and branch migration. Nucleic Acids Res, 2022, 50(20): 11727-11737. https://doi.org/10.1093/nar/gkac886

ARTICLE IN PRESS

[59] Zhang C, Cai Z, Zhou Z, et al. CASMART, a one-step CRISPR Cas12a-mediated isothermal amplification for rapid and high-resolution digital detection of rare mutant alleles. Biosens Bioelectron, 2023, 222, 114956. https://doi.org/10.1016/j.bios.2022.114956

ARTICLE IN PRESS

ARTICLE IN PRESS

Ethics and Consent to Participate declarations:

This study was approved by the Ethics Committee of Ningbo Clinical Pathology Diagnosis Center （approval number: NBPC-NBSZ202501）. As the study is an observational anonymous study, the signed informed consent was waived.

Acknowledgements

This work was supported by the Natural Science Foundation of Zhejiang Provincial (grant number LY23H260002), Public Welfare Technology Application Research Project of Ningbo (grant number 2023S106), Ningbo Top Medical and Health Research Program (grant number 2023010211), and K.C.Wong Magna Fund in Ningbo University.

CRediT authorship contribution statement

Tao ZHU: Data curation, Investigation, Methodology, Software, Writing - original draft. Zixuan WANG: Resources, Data curation. Yingyu WU: Software, Supervision. WeiWei JIANG: Supervision. Fei DENG: Methodology, Supervision. Rong FANG: Writing - Review and Editing, Resources, Funding acquisition. Danting YANG: Conceptualization, Methodology, Writing - Review and Editing, Supervision, Funding acquisition.

ARTICLE IN PRESS

Author statement

The authors declare that they have seen and approved the final version of the manuscript being submitted, and warrant that the article is the authors' original work, hasn't received prior publication and isn't under consideration for publication elsewhere. Permission has been received to use any material in the manuscript such as figures etc. which isn't original content.

Declaration of Competing Interest

The authors declare that they have no known competing financial interests or personal relationships that could have appeared to influence the work

ARTICLE IN PRESS

reported in this paper.

ARTICLE IN PRESS